# Measurement of γ rays from ^{15}N(p,γ)^{16}O cascade and ^{15}N(p,α_{1}γ)^{12}C reactions

G. Imbriani, R. J. deBoer, A. Best, M. Couder, G. Gervino, J. Görres, P. J. LeBlanc, H. Leiste, A. Lemut, E. Stech, F. Strieder, E. Uberseder, and M. Wiescher

Phys. Rev. C **85**, 065810 — Published 27 June 2012

DOI: 10.1103/PhysRevC.85.065810

# Measurement of $\gamma$-rays from $^{15}$N$(p,\gamma)^{16}$O cascade and $^{15}$N$(p,\alpha_1\gamma)^{12}$C reactions

G. Imbriani,[1,2] R. J. deBoer,[1,*] A. Best,[1] M. Couder,[1] G. Gervino,[3] J. Görres,[1] P. J. LeBlanc,[1] H. Leiste,[4] A. Lemut,[5] E. Stech,[1] F. Strieder,[6] E. Uberseder,[1] and M. Wiescher[1]

[1] *Department of Physics, University of Notre Dame, Notre Dame, Indiana 46556 USA*
[2] *Università degli Studi di Napoli "Federico II" and INFN, Napoli, Italy*
[3] *Università degli Studi di Torino and INFN, Torino, Italy*
[4] *Institut für Materialforschung I, Forschungszentrum Karlsruhe, Germany*
[5] *Università degli Studi di Genova and INFN, Genova, Italy*
[6] *Institut für Experimentalphysik, Ruhr-Universität Bochum, D-44780 Bochum, Germany*

**Background** The main energy production mechanism for massive stars during Hydrogen burning is the CNO cycle. The reactions $^{15}$N$(p,\gamma)^{16}$O and $^{15}$N$(p,\alpha_0)^{12}$C form a branch point in this cycle. The ratio of the corresponding reaction rates determines the CNO abundances evolving during this early stage of the star's life which affects the subsequent nucleosynthesis in later phases of stellar evolution. Determining the cross sections for these reactions at stellar energies is often very difficult. Measurements of other reactions that populate the same compound nucleus can often be used to indirectly determine the cross section of interest.

**Purpose** The nuclear level properties of broad resonances in $^{16}$O which characterize the cross section of the reactions $^{15}$N$(p,\gamma)^{16}$O and $^{15}$N$(p,\alpha_0)^{12}$C must be well known in order to accurately extrapolate the measured cross sections to the stellar energy range. The $R$-matrix formalism is a powerful technique for interpreting these cross sections and is greatly enhanced by additional data in other reaction channels. In a previous publication, measurements were reported for the cross section of the reaction $^{15}$N$(p,\gamma)^{16}$O for the ground state transition only. Concurrently, $\gamma$-ray measurements were recorded for the cascade transitions to the $E_x$ = 6.050, 6.130, and 7.117 MeV bound states of $^{16}$O as well as from the reaction $^{15}$N$(p,\alpha_1\gamma)^{12}$C. Excitation curves for the cascade transitions have never been measured and the excitation curve data for the $^{15}$N$(p,\alpha_1\gamma)^{12}$C reaction found in the literature may suffer from substantial errors due to target contamination.

**Methods** Angle integrated cross sections are measured over the proton energy range from $E_p$ = 0.14 to 1.80 MeV for the $\gamma$-ray cascade transitions and for the reaction $^{15}$N$(p,\alpha_1\gamma)^{12}$C.

**Results** De-excitations associated with several compound nucleus states in $^{16}$O are observed in both the $\gamma$-ray and $\alpha_1$-channels. An $R$-matrix analysis is performed and partial decay widths are deduced for several previously unobserved decay branchings from these states.

**Conclusion** For the first time, excitation curves for the cascade transitions to the $^{16}$O bound states at $E_x$ = 6.050, 6.130, and 7.117 MeV are reported over the energy range from $E_p$ = 0.14 to 1.80 MeV. In addition, an improved measurement of the $^{15}$N$(p,\alpha_1\gamma)^{12}$C excitation curve has been made over a similar energy range.

PACS numbers: Valid PACS appear here

## I. INTRODUCTION

During stellar Hydrogen burning in massive stars, the CNO cycle is the main source of energy production. Depending on the star's temperature, different branches of the CNO cycle become dominant, thereby affecting the star's later evolution. The reactions $^{15}$N$(p,\gamma)^{16}$O and $^{15}$N$(p,\alpha_0)^{12}$C form one such branch point between the CNO I and CNO II cycles (see, e.g., Refs. [1, 2]). Depending on the relative cross sections of the branch point reactions, different CNO abundances will emerge affecting, as seed material, the nucleosynthesis in subsequent phases of stellar evolution [3]. The temperatures of stellar Hydrogen burning correspond to low energy conditions. At these low energies, the reaction cross sections rapidly declines as a function of energy due to the Coulomb barrier. This makes direct measurement of these reactions impossible with existing techniques. Presently, measurements are made at higher energies where the cross sections are significantly larger. The higher energy cross sections are then extrapolated to the stellar energy range. The better the features of the low energy nuclear reaction mechanism are known, the more confident the extrapolation of the cross section becomes. For reactions like $^{15}$N+p, broad compound nucleus levels in $^{16}$O dominate the cross section. Populating these levels and observing multiple possible decay channels, provides information about all reaction channels contributing to the overall understanding of the decay mechanism. The current work presents original data for some of these levels, following the cascade decay channels into $^{16}$O and the $\alpha$-particle decay into the first excited state of $^{12}$C.

In a recent publication [4], new ground state transition data were presented for the $^{15}$N$(p,\gamma)^{16}$O reaction. Concurrently, $\gamma$-rays from $^{15}$N$(p,\gamma)^{16}$O cascade transitions to the $E_x$ = 6.050, 6.130, and 7.117 MeV bound states of $^{16}$O and from the $^{15}$N$(p,\alpha_1\gamma)^{12}$C reaction were measured but had not yet been reported. While the branching ratios for some of the cascade transitions have been reported previously [4–7], no cross section data has

*Electronic Address: rdeboer1@nd.edu

been published for individual transitions other than the ground state. In addition, Refs. [6, 8] have recently reported total cross sections for the reaction $^{15}$N$(p,\gamma)^{16}$O which may be compared with the sum of the ground state and cascade transitions.

The excitation functions for the $^{15}$N$(p,\alpha_1\gamma)^{12}$C have been measured before [7, 9–11], but the study presented here is based on significantly improved statistics compared to the previous data and shows less uncertainty associated with target contaminants. In particular, the data of Ref. [7] report the angle integrated cross section over the energy range of interest. However, the data are known to suffer from target contaminations [9] which may result in significant deviations from the true cross section. The reaction is therefore re-investigated in order to provide a more accurate and precise measurement.

In the following, the experimental setup described in Ref. [4] is briefly revisited, the cascade transitions and the $^{15}$N$(p,\alpha_1\gamma)^{12}$C data are presented, and an $R$-matrix analysis is described where the new data are fit simultaneously with the $^{15}$N$(p,\gamma_0)^{16}$O data and other previously reported data from the literature.

TABLE I: Previously observed states in the $^{16}$O compound nucleus over the energy range of the experimental data. Level energies and total widths from Ref. [14] are compared with those found using the $R$-matrix analysis of this work. The two narrow $2^-$ levels are observed in the data but are not fit in the analysis. Several of the energies are fixed in the analysis. Uncertainties are of the form $(statistical, systematic)$ where the statistical uncertainty arises from the counts of the yield data and the systematic uncertainty from the energy calibration of the accelerator [4].

| | $E_x$ (MeV) | | $\Gamma_{total}$ (MeV) | |
|---|---|---|---|---|
| $J^\pi$ | literature [14] | this work | literature [14] | this work |
| $1^-$ | 12.440(2) | 12.445 (1,1) | 91(6) | 98(1) |
| $2^-$ | 12.530(1)[a] | 12.530 (fixed) | 97(10)$\times10^{-3}$ | |
| $0^-$ | 12.796(4) | 12.796(2,1) | 40(4) | 52(3) |
| $2^-$ | 12.9686(4)[a] | 12.9686 (fixed) | 1.34(4) | |
| $2^+$ | 13.02(1) | 12.967(2,1) | 150(10) | 351(3) |
| $1^-$ | 13.090(8) | 13.090 (2,1) | 130(5) | 137(2) |
| $3^-$ | 13.129(10) | 13.142(1,1) | 110(30) | 95(1) |
| $3^-$ | 13.259(2) | 13.265 (fixed) | 21(1) | 24.8(5) |
| $1^+$ | 13.664(3) | 13.665(3,1) | 64(3) | 72(6) |

[a] narrow levels

## II. EXPERIMENT AND RESULTS

The measurements were performed at the University of Notre Dame's Nuclear Science Laboratory (NSL) and the LUNA facility at the National Laboratory of Gran Sasso (LNGS). Protons were accelerated to laboratory energies ranging from $E_p = 0.14$ to 1.80 MeV using a 1 MV JN and a 4 MV KN Van de Graaff accelerator at the NSL and a 400 kV Cockroft-Walton accelerator at LUNA [12]. Beam currents were kept at less than 10 $\mu$A at energies above 700 keV to limit the count rate from the $^{15}$N$(p,\alpha_1\gamma)^{12}$C reaction. At lower energies, beam currents as high as 20 $\mu$A were delivered to the target at the NSL and up to 200 $\mu$A at LUNA [13]. The $^{15}$N enriched TiN target used at the NSL was created by sputtering Ti onto Ta backings under a Nitrogen atmosphere enriched to 99.95 percent $^{15}$N. At LUNA, two targets were used, one with similar characteristics to that used at the NSL and another thicker target with a lesser isotopic enrichment of 83 percent. The thickness of all the targets was determined at the NSL by mapping the $^{15}$N$(p,\alpha_1\gamma)^{12}$C excitation curve in the vicinity of the narrow $2^-$ resonance at $E_p = 0.429$ MeV ($\Gamma = 97(10)$ eV [14]). The thickness of the target used for the NSL measurements was determined to be $7.2 \pm 0.3$ keV and the two targets used for the LUNA measurements were $9.5 \pm 0.4$ and $24.8 \pm 0.5$ keV. Over the course of the experiment at the NSL, the target thickness was monitored by scanning over the $E_p = 0.429$ MeV narrow resonance, no target degradation was observed. Because the $E_p = 0.429$ MeV was not accessible at LUNA, the $E_p = 0.338$ MeV resonance in $^{15}$N$(p,\gamma_0)^{16}$O was used to monitor the target thickness. Significant isotopic abundance of $^{14}$N in the thicker target used at LUNA enabled the use of the narrow $^{14}$N$(p,\gamma)^{15}$O resonance at $E_p = 0.278$ MeV to monitor the target stability. The higher beam currents used at LUNA resulted in substantial loss of target material which was monitored regularly and was later corrected for in the analysis. The target and the detector were mounted at 45° with respect to the incident beam direction. At the NSL, the reaction $\gamma$-rays were detected using a HPGe clover detector. At LUNA, a single crystal 115 percent HPGe detector was used. A detailed discussion of the experimental setup, targets, and detectors can be found in Ref. [4].

The measurements cover the excitation energy range in $^{16}$O from the proton separation energy at $E_x = 12.12741(1)$ [15] up to about $E_x = 14$ MeV. Previously reported levels in the compound nucleus over this excitation energy range are given in Table I. Between the two reactions under consideration, $^{15}$N$(p,\gamma)^{16}$O and $^{15}$N$(p,\alpha_1\gamma)^{12}$C, resonances associated with these levels may be observed. For the purpose of this analysis, it is useful to categorize the levels by their total widths $\Gamma_{total}$. Levels with $\Gamma_{total} < 25$ keV are considered narrow while those with $\Gamma_{total} > 25$ keV are considered broad. This distinction comes about for two reasons. The first is the effective energy thickness of the targets under consideration. The second is that this analysis is primarily concerned with the broad structure of the cross section. In this analysis, only the broad resonance structures are of interest. Only two of the levels in the energy region fall into the narrow category, the two $2^-$ levels at $E_x = 12.530$ and 12.9686. The recommended literature values for the energies and widths of these levels [14] are used to compare with the current data. Throughout the remainder of the text, the levels are referenced by the energies found in this analysis which are listed in Table I.

From the close geometry yields of the HPGe clover

detectors, cross sections have been determined relative to the well known cross sections of the $^{15}\mathrm{N}(p,\gamma)^{16}\mathrm{O}$ ground state transition [4] using the same efficiencies given shown in Fig. 5 of Ref. [4]. Because of the close geometry of the HPGe detectors, the observed yield covers a wide angular range and therefore corresponds very closely to the $4\pi$ angle integrated cross section. Based on the experimental angular distributions given in Ref. [9] and the geometrical Q-coefficients for the setup described in Ref. [4], it was calculated that the deviation between the measured cross section using the angular coverage of the detector setup should reproduce the actual $4\pi$ angle integrated $^{15}\mathrm{N}(p,\alpha_1\gamma)^{12}\mathrm{C}$ cross section to within an uncertainty of 4 percent.

For the cascade transitions, no previous angular distribution measurements have been made. In order to investigate the effects of the angular distribution, the angular distribution coefficients are calculated based on the resonant and direct contributions obtained in the $R$-matrix analysis described below. For the $E_x = 6.050$ MeV cascade, the angular distribution is isotropic since only decays from the two $1^-$ resonances are considered and the external capture component is assumed to be very small. The $E_x = 6.130$ MeV cascade is found to have the greatest uncertainty near the two $3^-$ levels at $E_x = 13.142$ and 13.265 MeV where the deviation reaches a maximum of 13 percent. For the $E_x = 7.117$ MeV cascade, the deviation is again found to be quite small, reaching a maximum of 3 percent deviation from isotropy.

The $^{15}\mathrm{N}(p,\gamma_0)^{16}\mathrm{O}$ data together with the cascade transition data to the $E_x = 6.050$, 6.130, and 7.117 MeV bound states are shown in Fig. 1 (labeled a) through d) respectively). The $^{15}\mathrm{N}(p,\alpha_1\gamma)^{12}\mathrm{C}$ data is shown in Fig. 2. The data have been transformed from cross section to astrophysical $S$-factor, as defined in Ref. [4], for more convenient viewing.

The $^{15}\mathrm{N}(p,\alpha_1\gamma)^{12}\mathrm{C}$ data was found to be in good agreement with most of the earlier excitation curve measurements [9–11]. In particular, the on-resonance cross sections determined for the broad $3^-$ and $1^+$ levels were in excellent agreement with those given in the literature as summarized in Table II.

The excitation function presented here, however, deviates substantially from the one presented in Ref. [7]. As noted previously [9], the excitation curve from Ref. [7] suffered from significant target contamination which appeared as cross section enhancements in non-resonant regions at energies just above strong resonances as can be seen in Fig. 3. These target contaminants were a result of the target preparation technique described in Ref. [16], where the enriched Nitrogen gas used in the evaporation process diffused into the Tantalum backings during the heating process.

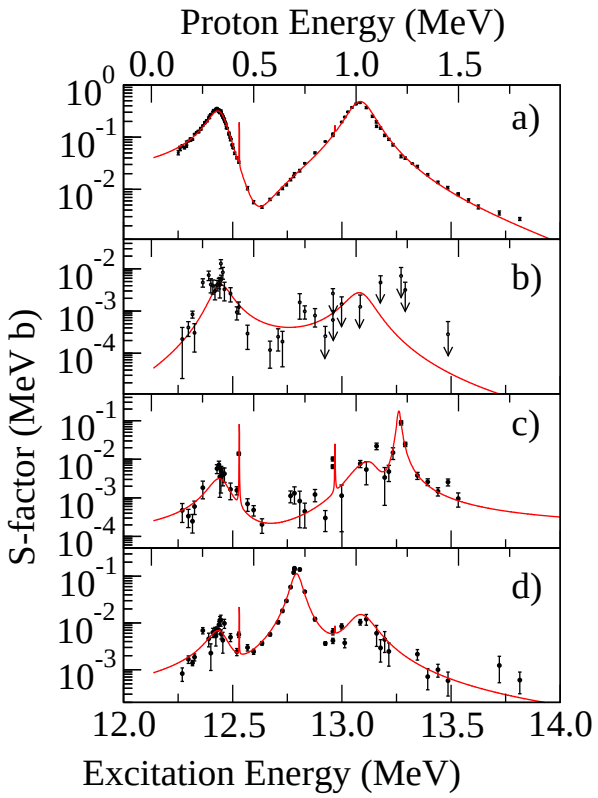


FIG. 1: (Color online) Simultaneous fits to the $^{15}\mathrm{N}(p,\gamma_0)^{16}\mathrm{O}$, $^{15}\mathrm{N}(p,\gamma_{(6.050)})^{16}\mathrm{O}$, $^{15}\mathrm{N}(p,\gamma_{(6.130)})^{16}\mathrm{O}$, and $^{15}\mathrm{N}(p,\gamma_{(7.117)})^{16}\mathrm{O}$ data of this work labeled a) through d) respectively. For the $E_x = 6.050$ transition, data points above $E_p = 0.85$ MeV are upper limits.

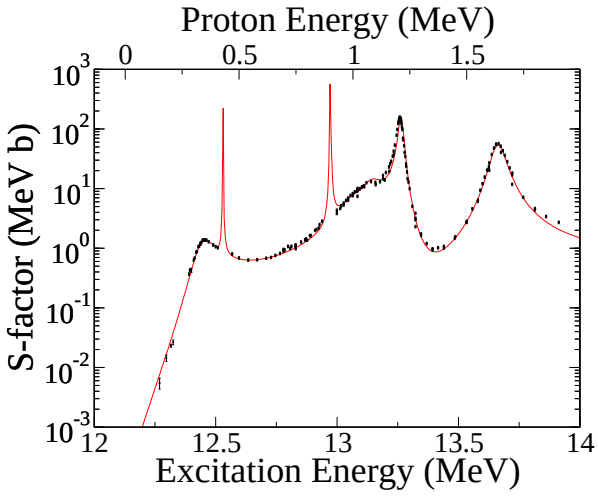


FIG. 2: (Color online) Fit to the $^{15}\mathrm{N}(p,\alpha_1\gamma)^{12}\mathrm{C}$ angle integrated cross section data of this work. Data in the region of the two narrow $2^-$ resonances have been omitted as large corrections for energy loss and straggling in the target would be required for an accurate fitting. The values for the energies and partial widths of the narrow resonances are fixed to those given in Ref. [14].

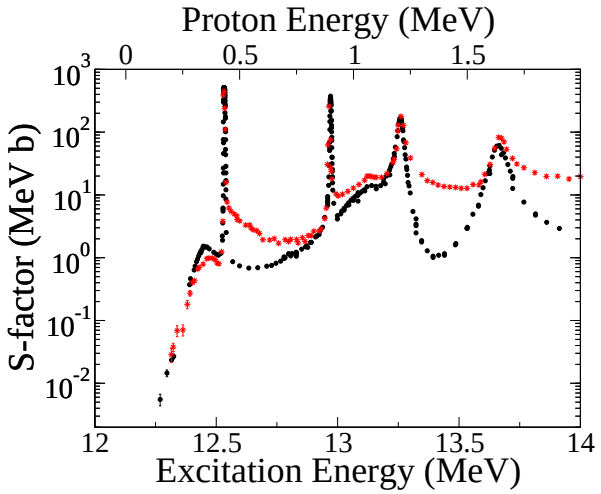


FIG. 3: (Color online) Comparison of the angle integrated $^{15}\mathrm{N}(p,\alpha_1\gamma)^{12}\mathrm{C}$ data of this work (black circles) to that of Ref. [7] (red stars). Nitrogen contamination in the backings of the targets of Ref. [7] are responsible for the overestimation of the cross section in non-resonant regions at energies just above strong resonances.

TABLE II: Comparison of on-resonance cross section measurements for the reaction $^{15}\mathrm{N}(p,\alpha_1\gamma)^{12}\mathrm{C}$. The uncertainties include a 5 percent uncertainty from the overall normalization to the $^{15}\mathrm{N}(p,\gamma)^{16}\mathrm{O}$ measurement and a combined uncertainty of 5 percent from the angular distribution effects and statistical uncertainty of the $^{15}\mathrm{N}(p,\alpha_1\gamma)^{12}\mathrm{C}$ data. Uncertainties for this work are presented in the form $(statistical, systematic)$.

| | | Cross Section (mb) | | |
|---|---|---|---|---|
| $E_x$ (MeV) | $J^\pi$ | this work | Ref. [11] | Ref. [9] |
| 13.265 | $3^-$ | 248(12,12) | 250(35) | 270(25) |
| 13.665 | $1^+$ | 166(8,8) | 190(15) | |

## III. ANALYSIS

The data have been analyzed in the framework of $R$-matrix theory [17] using a multiple channel approach where all reaction channels considered have been fit simultaneously [18]. The present code allows for the analysis of multiple entrance and exit channels. In addition to the data presented in this work, the analysis included several additional sets of literature data from other reaction channels [19, 20]. Because multiple particle decay channels are open over the entire energy region of the data, these additional reaction channel data are useful, and often necessary, in order to constrain the contributions to the total decay widths. $R$-matrix channel radii of 5.03 and 5.43 fm are used for the proton and $\alpha$-particle reaction channels respectively. Statistical uncertainties of the fit parameters are determined using the method described in Ref. [21] using the code MINUIT2 [22]. In cases of significant systematic uncertainties, both statistical and systematic uncertainties are quoted separately following the form $(statistical, systematic)$. Since these uncertainties are independent, the total uncertainty should be calculated by summing the contributions in quadrature.

While de-excitations from the two narrow $2^-$ resonances at $E_x = 12.530$ and 12.9686 MeV are observed in both the $^{15}\mathrm{N}(p,\alpha_1\gamma)^{12}\mathrm{C}$ and $^{15}\mathrm{N}(p,\gamma)^{16}\mathrm{O}$ cascade data, these levels are not included in the $R$-matrix analysis because large corrections for energy loss and straggling of the beam would be required. Further, the aim of the present analysis is to investigate the broad energy features of the cross section which are not effected by these levels.

Several resonances are observed in the $^{15}\mathrm{N}(p,\alpha_1\gamma)^{12}\mathrm{C}$ reaction channel. Three broad resonances are clearly observable in the data and correspond to previously observed levels in $^{16}$O at $E_x = 12.445$, 13.265, and 13.665 MeV with $J^\pi = 1^-$, $3^-$, and $1^+$ respectively. In addition, the levels at $E_x = 12.967$, 13.090, and 13.142 MeV with $J^\pi = 2^+$, $1^-$, and $3^-$ respectively also make significant contributions to the cross section.

The cascade transitions, shown in Fig. 1, indicate several resonant structures but because of the limited statistics and multiple possible resonance contributions, a unique resonance identification is sometimes difficult. Because multipolarity could not be determined from the data, possible assignments are adopted from the literature [14] whenever available. When no assignment has been reported, the lowest order multipolarity is adopted. Proton asymptotic normalization co-efficients (ANCs) have been measured for the $E_x = 6.130$ and 7.117 MeV transitions [23]. Since the data from this work do not provide a high level of constraint on the direct component of the cross section, the values of the ANCs are fixed to those resulting from transfer reaction measurement. Since the value of the ANC to the $E_x = 6.05$ MeV transition appears to be quite small, the direct component of the cross section is neglected for this transition.

All three cascade transitions display a resonance which is identified with the $E_x = 12.445$ MeV ($\mathrm{J}^\pi = 1^-$) state. In addition, the transition to the $E_x = 7.117$ MeV state clearly shows a resonance associated with the level at $E_x = 12.796$ MeV ($\mathrm{J}^\pi = 0^-$). Because of limited statistics, the higher energy data from the cascade transitions makes further resonance identification difficult. The data from the $E_x = 7.117$ MeV transition indicate a weak resonance associated with the $E_x = 13.090$ MeV ($\mathrm{J}^\pi = 1^-$) state. The partial width for this state is given in the literature [14] (see Table IV). Using the literature value for the partial width produces a cross section which is in reasonable agreement with the data.

The data corresponding to the transition to the $E_x = 6.130$ MeV state have some indication of transitions to two narrow resonances near $E_x = 12.53$ and 12.97 MeV which can be identified with the two $2^-$ states at $E_x = 12.530$ and 12.9686 MeV. Partial widths deduced from the branching ratios in the literature [14] are in reasonable agreement with the data. There is also a broad

structure near $E_x = 13.265$ MeV which can be well described by the $3^-$ resonance at the same energy. The data also indicate a broad structure near $E_x = 13$ MeV, which can be described most likely as a combination of the broad states, $3^-$ ($E_x = 13.142$ MeV, $\Gamma_{total} = 110(30)$ keV), $1^-$ ($E_x = 13.090$ MeV, $\Gamma_{total} = 130(5)$ keV), and $2^+$ ($E_x = 12.97$ MeV, $\Gamma_{total} = 150(10)$ keV), in this energy region. The broad $3^-$ ($E_x = 13.142$ MeV) and $1^-$ ($E_x = 13.090$ MeV) states can interfere with the other nearby resonances of the same $J^\pi$ ($J^\pi = 1^-$, $E_x = 12.445$ and $J^\pi = 3^-$, $E_x = 13.265$ MeV) to better reproduce the experimental cross section. The partial widths of these transitions to the $E_x = 6.130$ MeV bound state are fixed since their values are very weakly constrained. The contribution from the broad $2^+$ level at $E_x = 12.97$ MeV seems to be rather weak and its contribution to the $E_x = 6.130$ MeV transition is not included in the fit.

The cross section of the $E_x = 6.050$ MeV transition shows very little structure at energies above the $E_x = 12.445$ MeV ($J^\pi = 1^-$) state. Limited statistics resulted in only upper limits for data points above $E_p = 0.85$ MeV ($E_x = 12.92$ MeV). The literature reports a branching ratio of 0.58(12) for the $E_x = 13.090$ MeV ($J^\pi = 1^-$) state to this transition [14]. Based on the deduced partial width, a cross section is calculated that is consistent with the observed data. Therefore, the partial width of the $E_x = 6.050$ MeV transition is fixed at the value calculated from the ground state partial width of this work and the branching ratio in Ref. [14].

The $E_x = 6.050$ and 6.130 MeV excitation curves, shown in Fig. 1, both suggest some structure at about $E_x = 12.80$ MeV which also seems to be reflected in the transition to the $E_x = 7.117$ MeV state. This might suggest a contribution from the known $J^\pi = 0^-$ state at $E_x = 12.796$ MeV. However, the $E_x = 6.050$ MeV bound state has $J^\pi = 0^+$ making a $\gamma$-ray transition forbidden. A transition to the $E_x = 6.130$ MeV bound state is also quite unlikely since the state has $J^\pi = 3^-$ requiring an $M3$ transition. The origin and nature of these structures requires more detailed measurements.

The total $^{15}\mathrm{N}(p,\gamma)^{16}\mathrm{O}$ cross section data of Refs. [6, 8] can be compared to the sum of the cascade transitions and the ground state transition. The total cross section data span the the energy region from $E_p = 0.078$ to 0.393 MeV which extends to lower energy than the measurements presented here but does not cover the higher energy region. The shape of the total cross section data is found to be in good agreement with the sum of the ground state and cascade data as shown in Fig. 4. In order to match the scale of the sum of the current transition data, the total cross section data is multiplied by factors of 1.40 and 1.13 for the data presented in Refs. [6] and [8] respectively.

The results of the $R$-matrix calculation are shown by the solid red lines in Figs. 1 and 2. The $\alpha_1$ and $\gamma$-ray partial widths considered in the simultaneous fit to the $^{15}\mathrm{N}(p,\alpha_1\gamma)^{12}\mathrm{C}$ and the $^{15}\mathrm{N}(p,\gamma)^{16}\mathrm{O}$ cascade data are summarized in Tables III and IV. Table V lists the reduced $\chi^2$ values of the resulting fits.

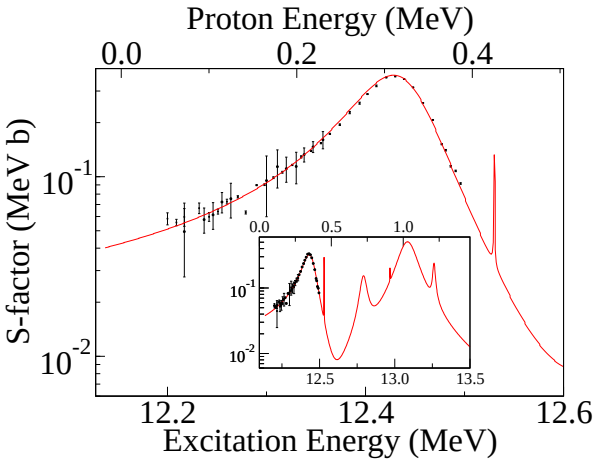


FIG. 4: (Color online) Comparison of the total $^{15}\mathrm{N}(p,\gamma)^{16}\mathrm{O}$ data of Refs. [6, 8] to the total $S$-factor calculated by summing the $R$-matrix fits from the cascade data of this work. The inset shows the extrapolation of the total $S$-factor over the full energy range of the present data. The data have been scaled to match that of the sum of the cascade data. See text for details.

TABLE III: Partial $\alpha_1$-widths for the states contributing to the $^{15}\mathrm{N}(p,\alpha_1\gamma)^{12}\mathrm{C}$ reaction data of this work. Those of the two $2^-$ resonances were fixed to the recommended values in the literature. The quoted uncertainties for this work are of the form $(statistical, systematic)$ where the statistical uncertainty arises from the counts of the yield data and the systematic uncertainty from the 5 percent absolute normalization of the cross sections [4]. Where the statistical uncertainty dominates, only that uncertainty is quoted.

| | | $\Gamma_{\alpha_1}$ (eV) | |
|---|---|---|---|
| $E_{x_i}$ (MeV) | $J^\pi$ | this work | Ref. [14] |
| 12.445 | $1^-$ | 30(2,2) | 25 |
| 12.530 | $2^-$ | fixed | 92(10) |
| 12.967 | $2^+$ | 500(200) | |
| 12.9686 | $2^-$ | fixed | 300(60) |
| 13.090 | $1^-$ | 580(40,30) | |
| 13.142 | $3^-$ | $20.9(6,10)\times10^3$ | $\sim20\times10^3$ |
| 13.265 | $3^-$ | $10.3(4,5)\times10^3$ | $8.2(11)\times10^3$ |
| 13.665 | $1^+$ | $64(6,3)\times10^3$ | $59(6)\times10^3$ |

The proton and $\alpha$ partial widths for each of the observed broad resonances are treated as a free parameter in the $R$-Matrix fit and are typically well constrained by data in other reaction channels as demonstrated in Refs. [19, 20]. The multichannel $R$-matrix analysis used here includes the data presented in Refs. [19, 20] and the literature data referenced therein. The proton and $\alpha$ partial widths given in Refs. [19, 20] are consistent with the values obtained in the current analysis and can be found in Table I of those works. A full description of the multichannel $R$-matrix fit will be presented in a forthcoming publication [24]. Implications for the determination of the low energy cross section of the $^{15}\mathrm{N}(p,\gamma)^{16}\mathrm{O}$ reaction

TABLE IV: Partial $\gamma$-widths for the resonance contributions to the $^{15}\mathrm{N}(p,\gamma_{(6.050)})^{16}\mathrm{O}$, $^{15}\mathrm{N}(p,\gamma_{(6.130)})^{16}\mathrm{O}$, and $^{15}\mathrm{N}(p,\gamma_{(7.117)})^{16}\mathrm{O}$ cascade reactions of this work. Multipolarities are taken from the literature when available, assumed values are enclosed in parentheses. Parameters which remain unconstrained by the data are fixed to those available in the literature. The quoted uncertainties for this work are of the form (*statistical*, *systematic*) where the statistical uncertainty arises from the counts of the yield data and the systematic uncertainty from the 5 percent absolute normalization of the cross sections [4]. Where the statistical uncertainty dominates, only one uncertainty is quoted.

| | | | | $\Gamma_{\gamma_i}$ (eV) | |
|---|---|---|---|---|---|
| $E_{x_i}$ (MeV) | $J^\pi$ | $E_{x_f}$ | $\Pi L$ | this work | Ref. [14] |
| 12.445 | $1^-$ | 6.050 | $E1$ | 0.09(4) | 0.12(6) |
| | | 6.130 | $(E2)$ | 0.07(3) | |
| | | 7.117 | $(M1)$ | 0.13(5) | |
| 12.530 | $2^-$ | 6.130 | $M1$ | fixed | 0.0162(25) |
| | | 7.117 | $M1$ | fixed | 0.0040(6) |
| 12.796 | $0^-$ | 7.117 | $M1$ | 2.7(2,2) | 2.5(2) |
| 12.9686 | $2^-$ | 6.130 | $M1$ | fixed | 0.0170(7) |
| | | 7.117 | $M1$ | fixed | 0.0020(4) |
| 13.090 | $1^-$ | 6.050 | $E1$ | fixed | 0.24(5) |
| | | 6.130 | $(E2)$ | 0.4(2) | |
| | | 7.117 | $M1$ | fixed | 1.35(4) |
| 13.142 | $3^-$ | 6.130 | $(M1)$ | 8[a] | |
| 13.265 | $3^-$ | 6.130 | $(M1)$ | 5(3) | |

[a]Very weakly constrained.

TABLE V: Reduced $\chi^2$ values resulting from the $R$-matrix analysis.

| Reaction | Reduced $\chi^2$ | Figure |
|---|---|---|
| $^{15}\mathrm{N}(p,\gamma_0)^{16}\mathrm{O}$ | 3.0 | 1a) |
| $^{15}\mathrm{N}(p,\gamma_{(6.050)})^{16}\mathrm{O}$ | 3.2 | 1b) |
| $^{15}\mathrm{N}(p,\gamma_{(6.130)})^{16}\mathrm{O}$ | 6.3 | 1c) |
| $^{15}\mathrm{N}(p,\gamma_{(7.117)})^{16}\mathrm{O}$ | 5.5 | 1d) |
| $^{15}\mathrm{N}(p,\alpha_1\gamma)^{12}\mathrm{C}$ | 8.2 | 2 |

and the resulting reaction rate based on the data presented here, in conjunction with other pre-existing data, will also be discussed.

## IV. CONCLUSION

Analysis of a particular reaction channel using the $R$-matrix technique can often greatly benefit from measurements in other reaction channels which share the same compound nucleus. The additional reaction channels provide both further constraints on the level parameters and a cross check of the different measurements. For the reaction $^{15}\mathrm{N}(p,\gamma_0)^{16}\mathrm{O}$, the reactions $^{15}\mathrm{N}(p,\alpha_1\gamma)^{12}\mathrm{C}$ and the $\gamma$-ray cascades are examples of these types of additional alternate channel reactions.

Previously, the only $^{15}\mathrm{N}(p,\alpha_1\gamma)^{12}\mathrm{C}$ data set available which covered a similar energy range of as the current $^{15}\mathrm{N}(p,\gamma)^{16}\mathrm{O}$ was that of Ref. [7]. Unfortunately, known target contaminations [9] present in the this data prevented it from being included in a multiple channel $R$-matrix analysis. In this paper, an improved measurement of the $^{15}\mathrm{N}(p,\alpha_1\gamma)^{12}\mathrm{C}$ excitation function is reported over a similar energy range, from $E_p = 0.14$ to 1.80 MeV, which is shown to be consistent with both the ground state $^{15}\mathrm{N}(p,\gamma)^{16}\mathrm{O}$ data of Ref. [4] and the concurrently measured cascade transition data. The cascade cross sections to the $^{16}$O bound states at $E_x = 6.050$, 6.130, and 7.117 MeV, measured for the first time, are reported over a similar energy range. Partial widths of states, corresponding to the resonances identified throughout the experimental energy region, have also been extracted for both the $\gamma$-ray cascade and the $\alpha_1$ channels. Both the cascade transitions and the $^{15}\mathrm{N}(p,\alpha_1\gamma)^{12}\mathrm{C}$ cross sections can be now be combined with other data in a multiple channel $R$-matrix framework for a better description of the $^{16}$O compound nucleus.

### Acknowledgments

The authors are grateful for the hospitality of the LNGS, the support of LNGS electronic and mechanical shops, and the LUNA collaboration. We thank R. E. Azuma for his contributions, numerous discussions, and critical remarks to the development of the $R$-matrix code. GI would like to acknowledge funding under MIUR Grant No. FIRB RBFR08549F. This work was funded by the National Science Foundation through Grant No. Phys-0758100, and the Joint Institute for Nuclear Astrophysics Grant No. Phys-0822648.

[1] C. Iliadis, *Nuclear Physics of Stars* (WILEY-VCH Verlag GmbH & Co. KGaA, Weinheim, 2007).
[2] M. Wiescher, J. Görres, E. Uberseder, G. Imbriani, and M. Pignatari, Annual Review of Nuclear and Particle Science **60**, 381 (2010).
[3] E. G. Adelberger, A. García, R. G. H. Robertson, K. A. Snover, A. B. Balantekin, K. Heeger, M. J. Ramsey-Musolf, D. Bemmerer, A. Junghans, C. A. Bertulani,

et al., Rev. Mod. Phys. **83**, 195 (2011).
[4] P. J. LeBlanc, G. Imbriani, J. Görres, M. Junker, R. Azuma, M. Beard, D. Bemmerer, A. Best, C. Broggini, A. Caciolli, et al., Phys. Rev. C **82**, 055804 (2010).
[5] F. Brochard, P. Chevallier, D. Disdier, V. Rauch, and F. Scheibling, Le Journal de Physique **34** (1973).
[6] D. Bemmerer, A. Caciolli, R. Bonetti, C. Broggini, F. Confortola, P. Corvisiero, H. Costantini, Z. Elekes, A. Formicola, Z. Fülöp, et al., Journal of Physics G: Nuclear and Particle Physics **36**, 045202 (2009).
[7] C. Rolfs and W. S. Rodney, Nuclear Physics A **235**, 450 (1974).
[8] Caciolli, A., Mazzocchi, C., Capogrosso, V., Bemmerer, D., Broggini, C., Corvisiero, P., Costantini, H., Elekes, Z., Formicola, A., Fülöp, Zs., et al., A&A **533**, A66 (2011).
[9] K. H. Bray, A. D. Frawley, T. R. Ophel, and F. C. Barker, Nuclear Physics A **288**, 334 (1977).
[10] F. B. Hagedorn and J. B. Marion, Phys. Rev. **108**, 1015 (1957).
[11] S. Bashkin, R. R. Carlson, and R. A. Douglas, Phys. Rev. **114**, 1543 (1959).
[12] H. Costantini, A. Formicola, G. Imbriani, M. Junker, C. Rolfs, and F. Strieder, Reports on Progress in Physics **72**, 086301 (2009).
[13] A. Formicola, G. Imbriani, M. Junker, D. Bemmerer, R. Bonetti, C. Broggini, C. Casella, P. Corvisiero, H. Costantini, G. Gervino, et al., Nuclear Instruments and Methods in Physics Research Section A: Accelerators, Spectrometers, Detectors and Associated Equipment **507**, 609 (2003), ISSN 0168-9002.
[14] D. R. Tilley, H. R. Weller, and C. M. Cheves, Nuclear Physics A **564**, 1 (1993).
[15] A. Wapstra, G. Audi, and C. Thibault, Nuclear Physics A **729**, 129 (2003).
[16] C. Rolfs, A. Charlesworth, and R. Azuma, Nuclear Physics A **199**, 257 (1973), ISSN 0375-9474.
[17] A. M. Lane and R. G. Thomas, Rev. Mod. Phys. **30**, 257 (1958).
[18] R. E. Azuma, E. Uberseder, E. C. Simpson, C. R. Brune, H. Costantini, R. J. de Boer, J. Görres, M. Heil, P. J. LeBlanc, C. Ugalde, et al., Phys. Rev. C **81**, 045805 (2010).
[19] R. J. deBoer, A. Couture, R. Detwiler, J. Görres, P. Tischhauser, E. Uberseder, C. Ugalde, E. Stech, M. Wiescher, and R. E. Azuma, Phys. Rev. C **85**, 045804 (2012).
[20] R. J. deBoer, P. J. LeBlanc, S. Falahat, G. Imbriani, J. Görres, S. O'Brien, E. Uberseder, and M. Wiescher, Phys. Rev. C **85**, 038801 (2012).
[21] P. Descouvemont, A. Adahchour, C. Angulo, A. Coc, and E. Vangioni-Flam, Atomic Data and Nuclear Data Tables **88**, 203 (2004).
[22] F. James and M. Winkler, *Minuit User's Guide* (2008).
[23] A. M. Mukhamedzhanov, P. Bém, V. Burjan, C. A. Gagliardi, V. Z. Goldberg, Z. Hons, M. La Cognata, V. Kroha, J. Mrázek, J. Novák, et al., Phys. Rev. C **78**, 015804 (2008).
[24] R. J. deBoer, E. Uberseder, J. Görres, G. Imbriani, P. J. LeBlanc, and M. Wiescher, Physical Review C, to be published (2012).